# Tuning Spin-Orbit Coupling and Superconductivity at the $SrTiO_3/LaAlO_3$ Interface: A Magnetotransport Study

M. Ben Shalom, M. Sachs, D. Rakhmilevitch, A. Palevski, and Y. Dagan*

*Raymond and Beverly Sackler School of Physics and Astronomy, Tel-Aviv University, Tel Aviv, 69978, Israel*

(Received 6 January 2010; published 26 March 2010)

The superconducting transition temperature $T_c$ of the $SrTiO_3/LaAlO_3$ interface was varied by the electric field effect. The anisotropy of the upper critical field and the normal-state magnetotransport were studied as a function of gate voltage. The spin-orbit coupling energy $\epsilon_{SO}$ is extracted. This tunable energy scale is used to explain the strong gate dependence of the mobility and of the anomalous Hall signal observed. $\epsilon_{SO}$ follows $T_c$ for the electric field range under study.

DOI: 10.1103/PhysRevLett.104.126802 PACS numbers: 73.40.−c, 74.25.F−, 74.62.−c

Interfaces between strongly correlated oxides exhibit a variety of physical phenomena and are currently at the focus of intensive scientific research. An electronic reconstruction occurring at the interfaces may be at the origin of these phenomena [1]. It has been demonstrated that the interface between $SrTiO_3$ (STO) and $LaAlO_3$ (LAO) is highly conducting, having the properties of a two-dimensional electron (2DEG) gas [2]. At low temperatures the 2DEG has a superconducting ground state, whose critical temperature can be modified by an electric field effect [3]. The origin of the charge carriers and the thickness of the conducting layers are still under debate [1,4–9]. Recently, we have demonstrated that for carrier concentrations at the range of $10^{13}$ $cm^{-2}$, a large, highly anisotropic magnetoresistance (MR) is observed [10]. Its strong anisotropy suggests that it stems from a strong magnetic scattering confined to the interface.

Here we show that both superconducting and spin-orbit (SO) interaction can be modified by applying a gate voltage. The upper critical field applied parallel to the interface, $H_{c2\|}$, is approximately the weak coupling Clogston-Chandrasekhar paramagnetic limit: $\sqrt{2}\mu_B H_{c2} \cong 1.75 k_B T_c$ for high carrier concentrations. However, as the carrier density is reduced, $H_{c2\|}$ becomes as large as 3.5 times this limit, suggesting a rapidly increasing SO coupling. This SO coupling energy $\epsilon_{SO}$ manifests itself in many of the transport properties studied.

We use a sample with 15 unit cells of LAO, deposited by pulsed laser on an atomically flat STO(100) substrate. Growth procedure is similar to the one described elsewhere [10]. A layer of gold was evaporated at the bottom of the sample and used as a gate when biased to $\pm 50$ V relative to the 2DEG. Contacts were made using a wire bonder in a van der Pauw geometry. Samples rotation was done using a step motor with a resolution of 0.015°/step. All transport properties reported here were measured in the as-grown state (AG), and while applying $V_g = 50, 10, -10, -50$ V. We took extra care to ensure the absence of heating and remnant magnetic fields.

Figure 1(a) presents the normalized resistance $R/R_n$ as a function of temperature for the various $V_g$ values. $R_n$ is the resistance measured at zero field and at $T = 0.5$ K, well above $T_c$, for each $V_g$. Tuning $V_g$ from $+50$ to $-50$ V increases $T_c$ from 0.1 to 0.35 K.

Figure 1(b) presents $R/R_n$ versus the perpendicular magnetic field at $T = 20$ mK. A large, positive MR is observed for $V_g = 50$ V. Its magnitude gradually decreases as $V_g$ is reduced. The inset zooms on the superconducting low field region.

Table I summarizes the transport properties for the various $V_g$. We define $H_{c2\perp}$ ($T_c$) as the field (temperature) at which the resistance is $R_n/2$. The Ginzburg Landau coherence length $\xi_{GL} = \sqrt{\Phi_0/2\pi\mu_0 H_{c\perp}}$ is extracted from $H_{c2\perp}$, here $\Phi_0$ is the flux quantum. The charge carrier density $n = 1/R_H e$ is inferred from Hall measurements at high fields ($\mu_0 H > 14$ T). It is presented together with the calculated mobility $\mu = n/R_n$. A large variation of $\mu$ is observed, indicating a significant change in the scattering rate with $V_g$ as previously noted [11]. This behavior will be discussed later.

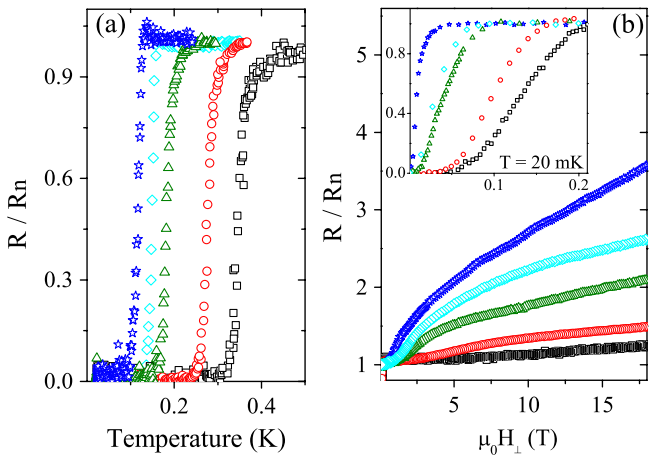


FIG. 1 (color online). (a) Normalized sheet resistance versus temperature for the various gate voltages (from left to right) $V_g = 50$ V, as-grown state, 10 V, $-10$ V, $-50$ V color and shape code applies to all graphs in the Letter. (b) Resistivity versus the perpendicular magnetic field. Inset: zoom on the low field region where superconductivity is suppressed.

 

TABLE I. Summary of the transport properties for various $V_g$.

| $V_g$ V | $n \times 10^{13}$ cm$^{-2}$ | Mobility cm$^2$/V s | $T_c$ K | $\mu_0 H c_\perp$ T | $\mu_0 H c_\parallel$ T | $d$ nm | $\xi_{GL}$ nm | $\epsilon_{SO}$ meV |
|---|---|---|---|---|---|---|---|---|
| −50 | 3.0 | 236 | 0.35 | 0.125 | 2.23 | 10 | 51 | >2 |
| −10 | 4.4 | 392 | 0.28 | 0.098 | 1.37 | 14.4 | 58 | 0.58 |
| 10 | 6.1 | 762 | 0.18 | 0.040 | 0.52 | 24.1 | 90 | 0.21 |
| 50 | 7.8 | 1707 | 0.12 | 0.009 | 0.14 | 41.2 | 194 | 0.06 |
| AG | 9.5 | 897 | 0.15 | 0.030 | 0.25 | 44 | 103 | 0.12 |

Figure 2 presents the sheet resistance versus the magnetic field $H_\parallel$, applied parallel to the interface and to the current. From the low field regime we extract the superconducting parallel critical field $H_{c2\parallel} = H(R_n/2)$. We note that while $T_c$ increases merely to 0.35 K, $H_{c2\parallel}$ becomes as large as 2.5 T [Table I]. The high $H_{c2\parallel}$ and low $T_c$ imply that the paramagnetic limit is exceeded [12]. Since $\xi_{GL}$ is rather large, 50–200 nm, it is reasonable to use the weak coupling BCS approximation. Accordingly, we expect superconductivity to exist in fields lower than $\sqrt{2} g \mu_B H \leq 3.5 k_B T_c$; here $g$ is the gyromagnetic ratio and $\mu_B$ is the Bohr magneton.

In Fig. 3(a) $\mu_B H_{c2\parallel}$ is plotted against $k_B T_c$ for different $V_g$ values. The dashed straight line represents the paramagnetic limit using BCS weak coupling and $g = 2$. As $T_c$ increases, the limit is exceeded by up to a factor of ~3.5. This behavior suggests a strong SO coupling that relaxes the Clogston-Chandrasekhar limitations [12]. For a superconducting layer thickness $d \ll \xi_{GL}$ it is expected that $H_{c2\parallel}$ be much larger than $H_{c2\perp}$. In this case the critical field is determined by the paramagnetic limit and the spin-orbit energy. From Fig. 3(a) it appears that except for the lowest $T_c$, superconductivity is quenched in this paramagnetic limit. We can therefore merely set an upper limit on the thickness of the conducting layer by analyzing the anisotropy of the critical field: $d \leq \sqrt{3}\Phi_0/\pi \xi_{GL} \mu_0 H_{c2\parallel}$ [13]. The thickness upper limit is presented for the various $V_g$ reaching a minimal value of 10 nm for $n = 3 \times 10^{13}$ cm$^{-2}$ [Table I]. Previous estimations obtained similar values. They, however, relate $d$ to the actual thickness [14,15].

Let us describe the general behavior of $R(H_\parallel)$ [Fig. 2] using the $n = 6.1 \times 10^{13}$ cm$^{-2}$ curve (green triangle) as an example. Above the superconducting transition, the sheet resistance reaches a roughly field-independent regime (0.9–1.8 T) in which the resistance approximately equals $R_n$. We define $H^*$ as the onset field where $dR/dH$ becomes negative. For $H > H^*$ the resistance drops to $R_{sat}$, the low resistance saturation regime ($H_\parallel > 10$ T). Both $H_{c2\parallel}$ and $H^*$ strongly depend on $V_g$; they increase as $V_g$ changes from 50 to −50 V, and $H^*$ becomes unmeasurably high for $V_g = -50$ V (black squares).

Figure 3(a) suggests that SO coupling plays a major role in the system. We shall now describe the data presented so far using a single energy scale $\epsilon_{SO}$. We relate $H^*$ to the breakdown field of the spin-orbit coupling energy: $g \mu_B H^* = \epsilon_{SO}$. The $\epsilon_{SO}$ values are presented assuming $g = 2$ [Table I]. Above this field SO scattering is sup-

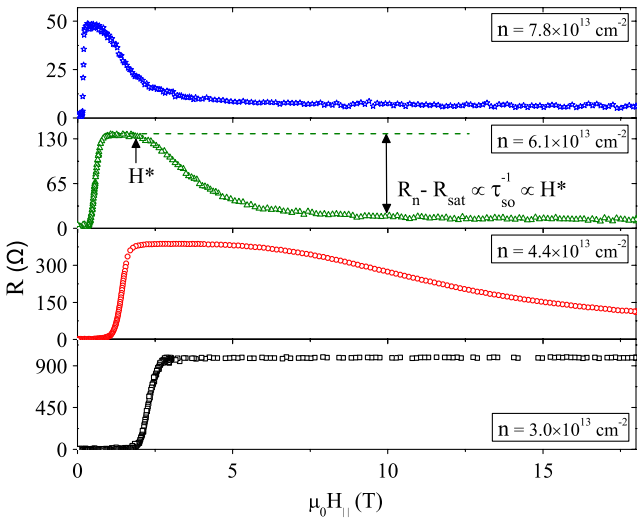


FIG. 2 (color online). Sheet resistance versus the magnetic field applied parallel to the interface and current for various charge densities.

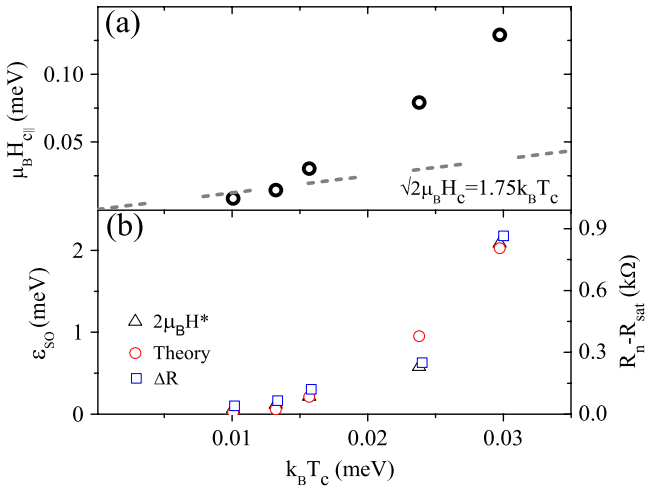


FIG. 3 (color online). (a) The parallel upper critical field $H_{c\parallel}$ versus $k_B T_c$ while $V_g$ is varied. The dashed line represents the expected behavior for the paramagnetic limit. (b) $\epsilon_{SO}$ extracted from $H^*$ [see Fig. 2], and calculated from the measured superconducting properties ($H_{c2\parallel}$ and $T_c$) [16], versus $k_B T_c$. The right axes presents $\Delta R$, which scales with $\epsilon_{SO}$ as expected.

pressed and completely vanishes at the high field saturation regime where all spins are aligned. In this scenario the high field saturation value $R_{sat}$ is the remnant impurity scattering. The SO scattering rate can be evaluated from the difference between $R_n$ and $R_{sat}$. Therefore $R_n$-$R_{sat}$ should be proportional to $h/\tau_{SO} = \epsilon_{SO}$.

Figure 3(b) presents $R_n$-$R_{sat}$ and $\mu_B H^*$ versus $k_B T_c$. These two quantities scale as predicted. Furthermore, the saturation resistance $R_{sat}$ roughly scales with the number of carriers. Since the spins do not align in the case of $V_g = -50$ V we estimate $\Delta R \sim R$ and give a lower bound for $H^*$. We further use the calculation of Klemm *et al.* which estimates the SO scattering time from $H_{c2\|}$ and $T_c$ for a two-dimensional film in the paramagnetic limit [16]. As seen [Fig. 3(b), red circles], the general behavior is described by this (probably oversimplified) model. We can therefore conclude that a single energy scale, tuned by $V_g$, dominates the behavior of the transport and affects superconductivity. For the carrier concentration range under study $R_{sat} \ll R_n$. Hence, the main contribution to the zero field resistance comes from SO scattering. This explains the strong dependence of mobility on $V_g$.

We note that for $V_g = 50$ V the carrier concentration is lower compared to the as-grown state. This is in contrast to a simple capacitorlike behavior with negative charge carriers. Furthermore, despite the decrease in carrier concentration, $R_n$ unexpectedly decreases. We relate this peculiar behavior to the SO scattering processes dominating $R_n$. We assume that static positive charges move to the interface when the highest positive voltage is applied and consequently $n$ is reduced. This charge movement reduces the initial electric field at the interface and as a result decreases the SO scattering. For this highest $V_g$ the paramagnetic limit is not exceeded indicating a smaller SO coupling. Upon reducing the gate voltage from its maximal positive value (as done in this experiment), electrons are drawn away from the interface in a reversible manner as expected, and an electric field is created. The initial electric field in the as-grown state results in enhanced SO scattering and higher resistance, despite the higher carrier concentration.

The MR presented [Figs. 1(b) and 2] is highly anisotropic for high magnetic fields. For example, for $n = 6.1 \times 10^{13}$ cm$^{-2}$ and $H = 18$ T, the resistance varies from $0.12R_n$ to $3.5R_n$ (a factor of 30) for the in-plane and out-of-plane field configurations, respectively. We study this anisotropy by rotating the sample around an in-plane axis which is perpendicular to the current, while keeping the total field constant, $|\vec{H}| = 18$ T. Figure 4(a) presents the normalized sheet resistance versus the perpendicular field component. For the small angle range presented, the parallel field component is approximately constant $\simeq$18 T. Moreover, for this parallel field component, the resistance is insensitive to small changes in $H_\|$ [Fig. 2]. As shown, the sheet resistance rapidly increases when a small perpendicular component is introduced. It reaches $R_n$ for $H_\perp \simeq 1.5$ T (an angle of about 4°). This is similar to our previous observation at 2 K [10]. The curves $n = 7.8$, $6.1 \times 10^{13}$ cm$^{-2}$ and AG (not shown) merge near 1.5 T, while $n = 4.4 \times 10^{13}$ cm$^{-2}$ departs form the general behavior. This can be easily explained since for this gate voltage the resistance does not saturate up to 18 T [Fig. 2]. For $n = 3.0 \times 10^{13}$ cm$^{-2}$, $H = 18$ T is well below $H^*$ and therefore the anisotropy cannot be observed at this too small a magnetic field.

Unlike the relatively small MR at low field in Fig. 1(b), in Fig. 4(a). there is an immediate increase in resistance upon applying a perpendicular field component. We relate this difference to the SO interaction. In this picture the band splits into two subbands with opposite chirality. This limits the orbital scattering. For $H_\| > H^*$ the spins are aligned and orbital scattering is not limited.

Figure 4(b) presents the Hall resistivity $\rho_{xy}$ at 20 mK versus the magnetic field after subtracting out the linear term obtained from a fit to the high field regime. A conspicuous deviation from this linear part in the Hall resistivity (anomalous Hall effect AHE), is observed. This AHE persists up to 100 K with a peculiar, roughly linear temperature dependence (not shown). As shown, the applied $V_g$ varies the AHE saturation field. This variation is inconsistent with a simple magnetic impurity scenario and with a simple ferromagnetic behavior. Furthermore, no hysteresis is observed for all carrier concentrations. Here we note that the AHE saturation field roughly follows the behavior of $\epsilon_{SO}$ and may be related to it.

Figure 4(c) compares the data in Fig. 4(b) in the case where $n = 4.4 \times 10^{13}$ cm$^{-2}$ (red circles), with data taken at constant magnetic field while rotating the sample [as in Fig. 4(a)]. For the rotation (brown pluses), the slope of the AHE is much steeper. The two measurements differ at low perpendicular fields where the mobility is an order of magnitude higher for the rotation. The qualitative variation between the measurements is expected since the AHE is usually proportional to some power of the resistivity. The AHE has been related to a multiple band structure (light and heavy) [11] and to incipient disordered magnetism induced by the field [17]. The former is unlikely in view of the strong AHE slope in the case of the rotation experiment. For the case of light and heavy charge carriers, one would expect the former to dominate the resistivity and the latter to dominate the low field Hall. However, both the resistivity and the AHE are very susceptible to a small perpendicular field.

Finally, we note that for the highest mobility state achieved (blue stars), quantum oscillations are observed in both MR and Hall measurements [Figs. 1(b) and 4(b)]. These oscillations will be analyzed separately [18].

SO interactions are expected to play a significant role at the interface due to the inversion symmetry breaking. The SO interaction term is of the form: $\epsilon_{SO} = \mathbf{p} \cdot \sigma \times \nabla V$ where $\mathbf{p}$ is the carrier momentum, $\sigma$ is the Pauli spinor, and $\nabla V$ is the electric field perpendicular to the interface in our system [19]. The strong gate dependence of $\epsilon_{SO}$ di-

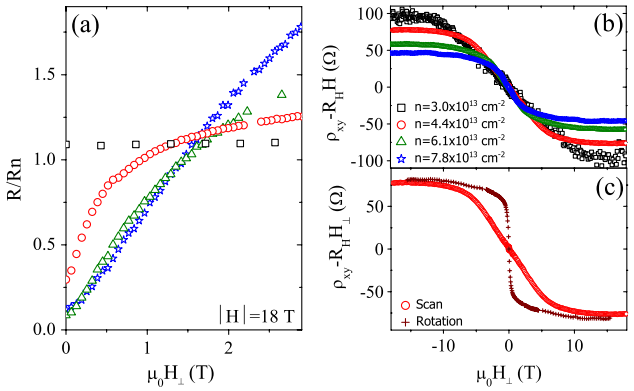


FIG. 4 (color online). (a) Normalized resistance as a function of perpendicular magnetic field. Data are taken while rotating the sample in a constant magnetic field of 18 T. (b) Hall resistivity after subtraction of a linear fit for high fields (AHE). (c) The AHE for $n = 4.4 \times 10^{13}$ cm$^{-2}$ while $H$ is scanned, and while rotating the sample at a constant field.

rectly follows from this expression. As pointed out above, the initial local electric field is unknown. When a positive gate voltage was applied for the first time the number of charge carriers decreased, while the resistivity decreased. We believe that this is mainly due to a decrease in the total electric field near the interface, resulting in a decreased SO scattering and an enhanced mobility. This suggests that the initial field (AG state) is a consequence of the electronic reconstruction. In this scenario, adding more LAO layers increases the as-grown field and hence the SO scattering. This explains the decrease in mobility while increasing the LAO thickness [20].

It seems that most scattering processes in the normal state involve a spin flip. Such processes strongly impede the transport. In a simple metal their contribution to the resistivity should be small. However, these processes become important in our system due to the strong SO coupling. This is clear in the case of in-plane spin flip processes; since SO coupling affects in-plane spin orientations, a spin flip process results in momentum reversal and consequently in a strong contribution to the resistivity. These spins are strongly coupled to the in-plane momenta; therefore it is impossible to align them with $H_{\|}$ unless the energy associated with the field $g\mu_B H_{\|}$ exceeds $\epsilon_{\mathrm{SO}}$. For $H > H^*$, the spins gradually align along the field direction and so $R_n$ is reduced. When all spins are aligned, the resistance reaches the saturation value $R_{\mathrm{sat}}$. For the out-of-plane field orientation, suppression of spin scattering is overwhelmed by the positive MR.

Tuning the $V_g$ from 50 to $-50$ V increases the local electric field, resulting in an increase of $\epsilon_{\mathrm{SO}}$ and $H^*$. Unlike $R_n$ (the zero field resistance), $R_{\mathrm{sat}}$ roughly scales with number of charge carriers deduced from the high field Hall measurements. This suggests that $R_{\mathrm{sat}}$ is a result of standard impurity scattering. For $V_g = -50$ V, $\epsilon_{\mathrm{SO}}$ is extremely large and an in-plane field of 18 T is not enough to align the spins and suppress the spin-scattering resistivity. Upon applying a small perpendicular field component and due to the large scattering time, orbital motion is immediately turned on along with the SO coupling. This results in a full recovery of the spin-MR.

In summary, we study the phase diagram of the $SrTiO_3/LaAlO_3$ interface in the region where $T_c$ increases while reducing the carrier concentration by variation of gate voltage [3]. We demonstrate the important effect of spin-orbit (SO) interaction on both superconductivity and on normal-state transport. The SO coupling energy ($\epsilon_{\mathrm{SO}}$) is evaluated using two independent transport properties, and is also in agreement with the theoretical model given the superconducting parameters: $T_c$ and the upper critical parallel field. $\epsilon_{\mathrm{SO}}$ follows $T_c$ for the electric field range studied. Our results suggest that oxide interfaces may be useful for future devices controlling the orbital motion of electrons by acting on their spins [21].

We are indebted to G. Deutscher, A. Aharony, E. Altman, J. Ruhman, and Ora Entin-Wohlman for enlightening discussions. This research was partially supported by ISF Grants No. 1543/08 and No. 1421/08 and by the Wolfson Family Charitable Trust. A portion of this work was performed at the National High Magnetic Field Laboratory, which is supported by NSF Cooperative Agreement No. DMR-0654118, by the state of Florida, and by the DOE. We thank J.-H. Park for his help at the magnet lab.

*yodagan@post.tau.ac.il

[1] S. Okamoto and A. J. Millis, Nature (London) **428**, 630 (2004).
[2] A. Ohtomo and H. Y. Hwang, Nature (London) **427**, 423 (2004).
[3] A. D. Caviglia *et al.*, Nature (London) **456**, 624 (2008).
[4] N. Nakagawa, H. Y. Hwang, and D. A. Muller, Nature Mater. **5**, 204 (2006).
[5] R. Pentcheva and W. E. Pickett, Phys. Rev. Lett. **102**, 107602 (2009).
[6] Z. S. Popović, S. Satpathy, and R. M. Martin, Phys. Rev. Lett. **101**, 256801 (2008).
[7] W. Siemons *et al.*, Phys. Rev. Lett. **98**, 196802 (2007).
[8] P. R. Willmott *et al.*, Phys. Rev. Lett. **99**, 155502 (2007).
[9] M. Basletic *et al.*, Nature Mater. **7**, 621 (2008).
[10] M. Ben Shalom *et al.*, Phys. Rev. B **80**, 140403(R) (2009).
[11] C. Bell *et al.*, Phys. Rev. Lett. **103**, 226802 (2009).
[12] A. M. Clogston, Phys. Rev. Lett. **9**, 266 (1962).
[13] J. P. Burger *et al.*, Phys. Rev. **137**, A853 (1965).
[14] N. Reyren *et al.*, Appl. Phys. Lett. **94**, 112506 (2009).
[15] Y. Kozuka *et al.*, Nature (London) **462**, 487 (2009).
[16] R. A. Klemm, A. Luther, and M. R. Beasley, Phys. Rev. B **12**, 877 (1975).
[17] S. Seri and L. Klein, Phys. Rev. B **80**, 180410(R) (2009).
[18] M. Ben Shalom *et al.* (to be published).
[19] Y. A. Bychkov and É. I. Rashba, JETP Lett. **39**, 78 (1984).
[20] C. Bell *et al.*, Appl. Phys. Lett. **94**, 222111 (2009).
[21] S. A. Wolf, Science **294**, 1488 (2001).